An Efficient Methodology to Analyze Plasma Edge Model Parameter Sensitivities

Maarten Blommaert[1], Detlev Reiter[2], Martine Baelmans[1]

Abstract

Quantifying uncertainties on code outputs is an important step for code-based design and scenario development. Because of the high computational cost of plasma edge transport simulations, the propagation of uncertainties on input parameters quickly becomes intractable. The paper starts with a short overview of current concepts to deal with this issue. A practical in parts adjoint approach to sensitivity calculation is then proposed for computationally efficient uncertainty propagation. The cumbersome derivation-by-hand of the sensitivity expressions is avoided, while the computational cost is roughly kept independent of the number of uncertain parameters. Sensitivities of the outer strike point temperature and a heat load objective are calculated for a WEST case. Transport coefficients, boundary condition parameters, rate coefficients, as well as uncertain parameters in the magnetic equilibrium calculation are considered. The sensitivities are verified to be accurate, while the computational cost to compute the entire sensitivity matrix is equivalent to only two plasma edge simulations. Furthermore, several logical trends are observed in the sensitivities.

Keywords: Plasma edge simulation, sensitivity calculation, continuous adjoint method

Email address: maarten.blommaert@kuleuven.be (Maarten Blommaert)

[1]KU Leuven, Department of Mechanical Engineering, 3001 Leuven, Belgium

[2]Institute of Energy and Climate Research (IEK-4), FZ Jülich GmbH, D-52425 Jülich, Germany

1. Introduction

Plasma edge transport codes such as B2-EIRENE [1] have been used intensively to assist ITER divertor design [2] and study operating scenarios [3]. Also for DEMO, these codes play an important role to guide extrapolation of current knowledge, gathered from experimental devices, to reactor-scale conditions [4]. Yet, while the model equations are deterministic, reactor operation is subject to a number of uncertainties that arise, such as manufacturing and control tolerances, and material property variations. Moreover, simulation results rely on a multitude of assumptions and are subject to errors associated to the applied numerics. Since the uncertainty on the code outputs is important information for designers, the question arises whether the impact of both uncertainties and modelling errors can be assessed.

Approaches to Uncertainty Quantification (UQ) consist of two main steps [5]. The first is the identification of uncertainty sources and the characterization of their statistical distribution. For example, the core input power in the Scrape-Off Layer (SOL) might for example be found to deviate from the chosen nominal value in experiments, according to a normal distribution with a given standard deviation. However, for some variables, like anomalous transport coefficients, a lack of knowledge might impede a full characterization. In those cases, a range of realistic values can still be constructed [5]. Also the model, its discretization, and numerical errors may be considered as uncertainties [5]. The second step consists of propagating these uncertainties through the model and analyzing their effect on the quantities of interest or *modelling objectives*. Different methods exist to propagate these uncertainties. The significant computational cost of CFD (Computational Fluid Dynamics), however, limits the applicability of several approaches [6]. In plasma edge studies, 1D parameter scans are traditionally exploited to characterize the influence of model input parameters (see e.g. [7]). However, for increasing numbers of uncertain parameters, a scan of the full parameter space quickly becomes intractable. A true approach to UQ for plasma edge simulations has therefore not been achieved.

In terms of computational resources, especially sensitivity-based methods are well-known for their efficiency in terms of computational effort [8]. One method called the *moment* method approximates the simulation objectives using a truncated Taylor expansion with respect to the uncertain parameters [6]. The validity of this approach is limited, though, to small parameter variations. An alternative is to use the sensitivities as a first analysis step

that eliminates the parameters with an insignificant influence in a two-step approach. Advanced approaches such as sensitivity-accelerated Monte Carlo approaches can finally be used to accurately examine the entire parameter space [8].

In these sensitivity-based methods, so-called *adjoint* sensitivity calculations are often exploited. These methods are characterized by a low computational cost, independent of the number of uncertain parameters. In plasma edge transport applications, adjoint based sensitivity calculations have shown to be very effective for optimal design of the divertor configuration [9, 10] and estimation of unknown model parameters [11]. The main disadvantage of the classical *adjoint approach* is that a significant amount of efforts is required for derivation and implementation. Using the adapted *in parts adjoint* method, elaborated in Ref. [12], these efforts can be significantly reduced.

This paper addresses the use of an in parts adjoint method as an efficient and flexible approach to calculate sensitivities of uncertain parameters. It may serve as a tool for sensitivity-based uncertainty propagation. In section 2, the method and its assets are described in comparison to the classical adjoint and finite difference approach. The method is then applied to study the parameter sensitivities in a plasma edge simulation of the WEST (Tungsten Environment in Steady-state Tokamak) divertor plasma [13, 14]. In section 3, the plasma edge model and set-up of this test case are described. The sensitivity results are presented and verified in section 4.

2. Parameter sensitivity calculation

Consider a plasma edge transport simulation with n input variables, formally combined in the vector $\boldsymbol{\varphi} = [\varphi_1, \varphi_2, \ldots, \varphi_\mathrm{n}]^\top$ and m simulation objectives, combined in the vector $\boldsymbol{\mathcal{I}} = [\mathcal{I}_1, \mathcal{I}_2, \ldots, \mathcal{I}_m]^\top$, as illustrated in figure 1. This input variable vector $\boldsymbol{\varphi}$ now includes all uncertain parameters. Examples of both uncertain parameters and simulations objectives will be given in section 3. Let $\boldsymbol{c}(\boldsymbol{\varphi}, \mathbf{q}) = 0$ represent the model equations and boundary conditions governing the plasma edge code of interest, with $\mathbf{q}$ a vector containing the plasma state variables, such as densities, velocities, and temperatures for which the equations are typically solved using an iterative and segregated solver. In general, the vector $\boldsymbol{\mathcal{I}}(\boldsymbol{\varphi}, \mathbf{q})$ thus depends on the input parameters $\boldsymbol{\varphi}$ both directly, and indirectly through the solution of the plasma equations $\boldsymbol{c}(\boldsymbol{\varphi}, \mathbf{q}) = 0$ for the plasma state $\mathbf{q}(\boldsymbol{\varphi})$. Formally, we can eliminate the model equations to define the reduced objective $\hat{\boldsymbol{\mathcal{I}}}(\boldsymbol{\varphi}) \equiv \boldsymbol{\mathcal{I}}(\boldsymbol{\varphi}, \mathbf{q}(\boldsymbol{\varphi}))$, see Eq.

(3) below. Sensitivity-based UQ methods then exploit the derivative matrix $d\hat{\boldsymbol{\mathcal{I}}}/d\boldsymbol{\varphi}$ as a tool to calculate the uncertainty on the simulation objective vector $\boldsymbol{\mathcal{I}}$.

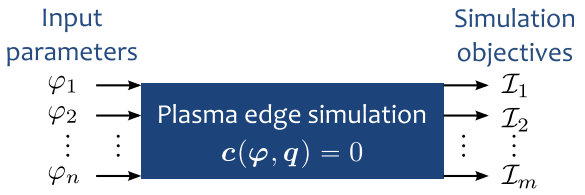

Figure 1: A conceptual representation of the code with input vector $\boldsymbol{\varphi}$, model equations $\boldsymbol{c}(\boldsymbol{\varphi}, \mathbf{q}) = 0$, and simulation objective vector $\hat{\boldsymbol{\mathcal{I}}}(\boldsymbol{\varphi})$.

In this section, the finite difference and adjoint approach to sensitivity calculations are summarized, and their assets and flaws are discussed. Subsequently, the recently developed in parts adjoint approach will be explained.

2.1. Finite difference approximation

The finite difference approach is by far the simplest approach to calculate the sensitivity of simulation objectives with respect to the uncertain parameters. However, it is part of a class of approaches of the *forward* type, for which the computational cost scales with the number of input parameters n. For each parameter φ_i, the (forward) finite difference formula approximates the directional derivative $d\hat{\boldsymbol{\mathcal{I}}}/d\boldsymbol{\varphi}\ \boldsymbol{\delta\varphi}_i$ as

$$\frac{d\hat{\boldsymbol{\mathcal{I}}}}{d\boldsymbol{\varphi}}(\boldsymbol{\varphi}_0)\,\boldsymbol{\delta\varphi}_i \approx \frac{\hat{\boldsymbol{\mathcal{I}}}(\boldsymbol{\varphi}_0 + \epsilon\boldsymbol{\delta\varphi}_i) - \hat{\boldsymbol{\mathcal{I}}}(\boldsymbol{\varphi}_0)}{\epsilon}, \tag{1}$$

with $\boldsymbol{\delta\varphi}_i$ a perturbation vector of length n in which only the i^{th} component is nonzero and $\boldsymbol{\varphi}_0$ the parameters at which the sensitivity is to be evaluated. To evaluate the entire derivative matrix $d\hat{\boldsymbol{\mathcal{I}}}/d\boldsymbol{\varphi}$, expression (1) has to be evaluated with n different vectors $\boldsymbol{\delta\varphi}_i$. Including the reference simulation, $n+1$ evaluations of the plasma edge code are needed for the finite difference calculation of the entire derivative matrix. Or equivalently:

$$\text{CPU-cost}(\frac{d\hat{\boldsymbol{\mathcal{I}}}}{d\boldsymbol{\varphi}}) \approx (n+1)\ \text{CPU-cost}(\hat{\boldsymbol{\mathcal{I}}}(\boldsymbol{\varphi})). \tag{2}$$

Higher order finite difference approximations can be used to reduce the truncation error but increase the number of code evaluations needed. Since the finite difference formula simply uses the original plasma edge code for the evaluation of the state variables $\mathbf{q}(\boldsymbol{\varphi}_0)$ and perturbed state variables $\mathbf{q}(\boldsymbol{\varphi}_0 + \epsilon\boldsymbol{\delta\varphi}_i)$, application of the method is straightforward. This is also the main asset of the method.

2.2. Adjoint approach

In adjoint approaches to sensitivity calculation, one distinguishes between so-called *continuous adjoint* and *discrete adjoint* approaches [15]. The first method is based on the adjoint formulation of the continuous equations $\boldsymbol{c}(\boldsymbol{\varphi}, \mathbf{q}) = 0$ and then discretized, while the second one applies the adjoint method to their spatially discretized approximation. The latter will be conveniently denoted by the same expression here. Conceptually, the derivations are similar, though the continuous adjoint requires a treatment in function spaces, which slightly complicates notation. To focus on the concept, we will only outline the discrete adjoint approach here. The reader is referred to Ref. [12] for a derivation of the continuous adjoint and in parts continuous adjoint procedures to sensitivity calculation.

One possible derivation of the adjoint procedure starts from the chain rule:

$$\frac{d\hat{\boldsymbol{\mathcal{I}}}}{d\boldsymbol{\varphi}} = \frac{\partial \boldsymbol{\mathcal{I}}}{\partial \boldsymbol{\varphi}} + \frac{\partial \boldsymbol{\mathcal{I}}}{\partial \mathbf{q}} \frac{d\mathbf{q}}{d\boldsymbol{\varphi}}. \tag{3}$$

Especially the derivative $d\mathbf{q}/d\boldsymbol{\varphi}$ is expensive to calculate for a large number of parameters n. After running the code to solve the model equations for $\mathbf{q}_0 = \mathbf{q}(\boldsymbol{\varphi}_0)$, the model equations $\boldsymbol{c}(\boldsymbol{\varphi}, \mathbf{q}) = 0$ can be linearized at $(\boldsymbol{\varphi}_0, \mathbf{q}_0)$ to find an expression for this derivative,

$$\frac{d\mathbf{q}}{d\boldsymbol{\varphi}} = -\left(\frac{\partial \boldsymbol{c}}{\partial \mathbf{q}}\right)^{-1} \frac{\partial \boldsymbol{c}}{\partial \boldsymbol{\varphi}}. \tag{4}$$

Substituting (4) in (3) and rearranging then leads to the expression

$$\frac{d\hat{\boldsymbol{\mathcal{I}}}}{d\boldsymbol{\varphi}} = \frac{\partial \boldsymbol{\mathcal{I}}}{\partial \boldsymbol{\varphi}} + \left[-\left(\frac{\partial \boldsymbol{c}}{\partial \mathbf{q}}\right)^{-\top} \left(\frac{\partial \boldsymbol{\mathcal{I}}}{\partial \mathbf{q}}\right)^{\top}\right]^{\top} \frac{\partial \boldsymbol{c}}{\partial \boldsymbol{\varphi}},$$

with the operator $(\cdot)^{-\top} = \left[(\cdot)^{-1}\right]^{\top} = \left[(\cdot)^{\top}\right]^{-1}$ denoting the inverse of the transpose. The adjoint approach then consists in substituting the expression

between brackets by the vector of adjoint state variables $\mathbf{q}^*$, solved from the adjoint equations

$$\left(\frac{\partial \boldsymbol{c}}{\partial \mathbf{q}}\right)^\top \mathbf{q}^* = -\left(\frac{\partial \boldsymbol{\mathcal{I}}}{\partial \mathbf{q}}\right)^\top. \tag{5}$$

Once the adjoint variables $\mathbf{q}_0^* = \mathbf{q}^*(\boldsymbol{\varphi}_0, \mathbf{q}_0)$ are calculated, the derivative matrix evaluates as

$$\frac{d\hat{\boldsymbol{\mathcal{I}}}}{d\boldsymbol{\varphi}}(\boldsymbol{\varphi}_0) = \frac{\partial \boldsymbol{\mathcal{I}}}{\partial \boldsymbol{\varphi}}(\boldsymbol{\varphi}_0, \mathbf{q}_0) + (\mathbf{q}_0^*)^\top \frac{\partial \boldsymbol{c}}{\partial \boldsymbol{\varphi}}(\boldsymbol{\varphi}_0, \mathbf{q}_0), \tag{6}$$

in which only derivatives of $\boldsymbol{\mathcal{I}}$ and $\boldsymbol{c}$ to the direct occurrence of $\boldsymbol{\varphi}$ remain. These derivatives are typically obtained by linearizing objective and equations by hand and evaluating the expressions.

The main computational cost of the sensitivity evaluation is therefore the cost of solving the adjoint equation (5). Although the adjoint system of equations is linear in $\mathbf{q}^*$, obtaining the exact linearization $\partial \boldsymbol{c}/\partial \mathbf{q}$ is almost never achievable in practice. In the continuous adjoint approach, the similarity between model and adjoint equations is therefore often exploited to construct a segregated solver for the adjoint equations and solve the equations using the same numerical routines as the forward simulation itself (see e.g. Ref. [16]). Due to this reason, the solution of the system of adjoint equations requires about the same CPU-cost as the forward simulation for each right-hand side $-\left(\partial \mathcal{I}_i/\partial \mathbf{q}\right)^\top$. The adjoint method is thus characterized by a computational cost,

$$\text{CPU-cost}\left(\frac{d\hat{\boldsymbol{\mathcal{I}}}}{d\boldsymbol{\varphi}}\right) \approx (m+1)\ \text{CPU-cost}(\hat{\boldsymbol{\mathcal{I}}}(\boldsymbol{\varphi})), \tag{7}$$

which scales with the number of simulation objectives m, but is independent of the number of parameters n. When designing components, the amount of quantities of interest is often a lot lower than the number of uncertain parameters. The method then features a significant reduction of computational cost with respect to forward methods. The linearization by hand of the partial derivatives in equations (5) and (6) and their implementation, however, requires a substantial amount of efforts.

2.3. In parts adjoint approach

The in parts adjoint approach attempts to exploit the efficiency of the adjoint approach, while reducing development efforts. Again, model equations and the adjoint equations for (5) are solved first. But now the partial

derivatives with respect to the uncertain parameters in the sensitivity expression of equation (6) are no longer evaluated by hand. Instead, the directional derivative $d\hat{\boldsymbol{\mathcal{I}}} \Big/ d\boldsymbol{\varphi}\ \boldsymbol{\delta\varphi}_i$ at the reference parameters $\boldsymbol{\varphi}_0$ is approximated using the central finite difference approximation

$$\begin{aligned}\frac{d\hat{\boldsymbol{\mathcal{I}}}}{d\boldsymbol{\varphi}}(\boldsymbol{\varphi}_0)\boldsymbol{\delta\varphi}_i \approx & \frac{\boldsymbol{\mathcal{I}}(\boldsymbol{\varphi}_0+\epsilon\boldsymbol{\delta\varphi}_i,\mathbf{q}_0)-\boldsymbol{\mathcal{I}}(\boldsymbol{\varphi}_0-\epsilon\boldsymbol{\delta\varphi}_i,\mathbf{q}_0)}{2\epsilon} \\ & + (\mathbf{q}_0^*)^\top \frac{\boldsymbol{c}(\boldsymbol{\varphi}_0+\epsilon\boldsymbol{\delta\varphi}_i,\mathbf{q}_0)-\boldsymbol{c}(\boldsymbol{\varphi}_0-\epsilon\boldsymbol{\delta\varphi}_i,\mathbf{q}_0)}{2\epsilon}.\end{aligned} \tag{8}$$

It should be noted that these perturbed objective and constraint vectors, $\boldsymbol{\mathcal{I}}$ and $\boldsymbol{c}$, respectively, are evaluated at constant $\mathbf{q}$. Therefore, the expression can still be evaluated at low CPU-cost. In practice, evaluating $\boldsymbol{c}(\boldsymbol{\varphi}_0+\epsilon\boldsymbol{\delta\varphi}_i,\mathbf{q}_0)$ means evaluating the discrete residuals of the equations at the converged plasma state, while the i^{th} uncertain variable is perturbed.

Although expression (8) needs to be evaluated n times to obtain the entire derivative matrix, the low computational cost of this evaluation does barely add on that of the forward and adjoint simulations. The method therefore features the efficiency of the adjoint method, while avoiding additional derivational work if a new parameter is added. Only the adjoint equations themselves need to be derived and implemented. Once in place, the in parts adjoint framework offers a pragmatical alternative to calculate the sensitivity matrix. For a single simulation objective, the user then only needs to spend an additional computational cost equivalent to one forward simulation, to easily determine the sensitivity towards all code parameters of interest.

Although the formula is derived here is derived here for the discrete adjoint method, a similar expression is found when elaborating on the continuous adjoint framework. A consistent choice between the continuous boundary conditions in the derivation and their discrete implementation is then, however, crucial.

3. Test case description

We now apply the in parts adjoint calculation of model parameter sensitivities to a slightly reduced plasma edge model in comparison to the hybrid fluid-kinetic B2-EIRENE code [1]. The WEST case of Ref. [12] is used with parameters similar to those of the SOLEDGE2D-EIRENE simulation of the "far" configuration in Ref. [17]. Here, we will only give the main model characteristics.

3.1. Model

The plasma edge transport model features a single species plasma with ion mass m and charge state Z_i in a poloidal cross section of a toroidally symmetric tokamak. Particle and momentum equations are solved for the ion density n_i and ion parallel velocity $u_\parallel$. The neutral pressure p_n is determined by an isotropic pressure diffusion equation. The heat flow is described by an overall internal energy equation that is solved for a combined ion-electron-neutral temperature $T = T_\mathrm{i} = T_\mathrm{e} = T_\mathrm{n}$. The vector of plasma state variables then becomes $\mathbf{q} = \left[n_\mathrm{i}, u_\parallel, T, p_\mathrm{n}\right]^\top$. The plasma edge transport is described by a set of partial differential equations, expressed in a curvilinear coordinate system that is aligned to the contours of the poloidal magnetic flux ψ and given by:

$$\begin{aligned}\boldsymbol{\mathcal{B}}(\boldsymbol{\varphi}, \psi, \mathbf{q}) = S(\boldsymbol{\varphi}, \psi, \mathbf{q}) - \frac{1}{\sqrt{g}}\frac{\partial}{\partial\theta}\left(\frac{\sqrt{g}}{h_\theta}C^\theta(\psi, \mathbf{q}) - \frac{\sqrt{g}}{h_\theta^2}D^\theta(\boldsymbol{\varphi}, \psi, \mathbf{q})\frac{\partial\mathbf{q}}{\partial\theta}\right) \\ + \frac{1}{\sqrt{g}}\frac{\partial}{\partial r}\left(\frac{\sqrt{g}}{h_r^2}D^r(\boldsymbol{\varphi}, \psi, \mathbf{q})\frac{\partial\mathbf{q}}{\partial r}\right) = 0,\end{aligned} \tag{9}$$

with $C^\theta(\psi, \mathbf{q}) = \left[n_\mathrm{i}u_\theta, mn_\mathrm{i}u_\theta u_\parallel, \frac{5}{2}\left(1 + Z_\mathrm{i}\right)n_\mathrm{i}u_\theta T, 0\right]^\top$ the convective poloidal fluxes, with $u_\theta = b_\theta u_\parallel$ the ion poloidal velocity and b_θ the poloidal magnetic field pitch. $D^\theta(\boldsymbol{\varphi}, \psi, \mathbf{q}) = \mathrm{diag}(0, \eta_\theta^\mathrm{i}, \kappa_\theta, D_p^\mathrm{n})$ is a matrix containing the the poloidal transport coefficients according to Braginskii [18], with $\kappa_\theta = \kappa_\theta^\mathrm{i} + \kappa_\theta^\mathrm{e} + \kappa^\mathrm{n}$ the total poloidal conductive coefficient and with the neutral conductivity given by $\kappa^\mathrm{n} = \chi^\mathrm{n}p_\mathrm{n}D_p^\mathrm{n}$. The radial transport is purely anomalous and leads to the matrix

$$D^r(\boldsymbol{\varphi}, \mathbf{q}) = \begin{pmatrix} D^\mathrm{i} & 0 & 0 & 0 \\ mD^\mathrm{i}u_\parallel & \eta_r^\mathrm{i} & 0 & 0 \\ \frac{5}{2}\left(1 + Z_\mathrm{i}\right)D^\mathrm{i}T & 0 & \kappa_r & 0 \\ 0 & 0 & 0 & D_p^\mathrm{n} \end{pmatrix}.$$

The radial transport coefficients for ion viscosity $\eta_r^\mathrm{i} = \nu^\mathrm{i}mn_\mathrm{i}$ and transverse conductivity $\kappa_r = \kappa_r^\mathrm{i} + \kappa_r^\mathrm{e} + \kappa^\mathrm{n}$, with $\kappa_r^\mathrm{i} = \chi^\mathrm{i}n_\mathrm{i}$ and $\kappa_r^\mathrm{e} = \chi^\mathrm{e}Z_\mathrm{i}n_\mathrm{i}$, contain the coefficients ν^i, χ^i, χ^e, and χ^n that are typically calibrated from experiments or turbulence models. The neutral pressure diffusion coefficient D_p^n is based on a balance between pressure gradient force and momentum source terms [19] and reads

$$D_p^\mathrm{n} = \frac{1}{m\left(n_\mathrm{i}K_\mathrm{cx} + n_\mathrm{e}K_\mathrm{i}\right)}.$$

The source terms are combined in the vector

$$S(\boldsymbol{\varphi}, \psi, \mathbf{q}) = \begin{pmatrix} n_\mathrm{e} n_\mathrm{n} K_\mathrm{i} - n_\mathrm{i} n_\mathrm{e} K_\mathrm{r} \\ -\frac{b_\theta}{h_\theta} \frac{\partial p}{\partial \theta} - m n_\mathrm{i} n_\mathrm{e} K_\mathrm{r} u_\parallel - m n_\mathrm{i} n_\mathrm{n} K_\mathrm{cx} u_\parallel \\ -E_\mathrm{i} n_\mathrm{e} n_\mathrm{n} K_\mathrm{i} \\ n_\mathrm{i} n_\mathrm{e} K_\mathrm{r} - n_\mathrm{e} n_\mathrm{n} K_\mathrm{i} \end{pmatrix},$$

with $n_\mathrm{n} = p_\mathrm{n}/T$ the neutral density and $p = (1+Z_\mathrm{i}) n_\mathrm{i} T$ the plasma pressure. Analytical expressions are used to approximate rate coefficients $K_\mathrm{i}, K_\mathrm{r}$, and K_cx for electron impact ionization [20], radiative recombination [20], and charge-exchange [21], respectively:

$$K_\mathrm{i} = \frac{2.0 \cdot 10^{-13}}{6.0 + \frac{T_\mathrm{e}(\mathrm{eV})}{13.6}} \left(\frac{T_\mathrm{e}(\mathrm{eV})}{13.6} \right)^{\frac{1}{2}} \exp\left(-\frac{13.6}{T_\mathrm{e}(\mathrm{eV})} \right),$$

$$K_\mathrm{r} = 0.7 \cdot 10^{-19} \left(\frac{13.6}{T_\mathrm{e}(\mathrm{eV})} \right)^{\frac{1}{2}}, \qquad K_\mathrm{cx} = 3.2 \cdot 10^{-15} \sqrt{\frac{T_\mathrm{i}(\mathrm{eV})}{0.025}}.$$

This plasma edge model is complemented with a set of boundary conditions $\boldsymbol{\mathcal{B}} = 0$, described in [12]. At the core boundary, heat flux ($Q_\mathrm{c} = 7.93\,\mathrm{MW}$) and plasma density ($n_\mathrm{c} = 1.3 \cdot 10^{19}\,\mathrm{m}^{-3}$) are specified. At the outer radial boundaries, particle and energy decay lengths, $\lambda_n = 0.05\,\mathrm{m}$ and $\lambda_T = 0.3\,\mathrm{m}$, determine the ion and energy flux over the last simulated flux line. Together, domain and boundary condition contributions form the plasma edge state equations $\boldsymbol{c}_\mathrm{pe} = (\boldsymbol{\mathcal{B}}, \boldsymbol{\mathcal{C}})^T = 0$.

The model additionally includes a free boundary magnetic equilibrium (FBE) code [22]. In the core region, this FBE code solves the Grad-Shafranov equation [23, 24]

$$-R\,\nabla \cdot \left(\frac{1}{\mu_0 R^2} \nabla \psi \right) = R p^{'}(\psi) + 1/(\mu_0 R)\; F F^{'}(\psi), \tag{10}$$

with $p(\psi)$ and $F(\psi)$ flux functions related to the plasma pressure and toroidal magnetic field, respectively. These profiles are parametrized using the profile parameters α, β, γ and given in the form [25]

$$p^{'}(\psi) = \lambda \frac{\beta}{R_0} (1 - \bar{\psi}^\alpha)^\gamma \quad \text{and} \quad F F^{'}(\psi) = \lambda (1-\beta) \mu_0 R_0 (1 - \bar{\psi}^\alpha)^\gamma,$$

with λ a scaling coefficient to comply with a preset total toroidal current I_P, and $\bar{\psi}$ the normalized magnetic flux, which equals 0 at the magnetic axis and 1 at the core boundary.

3.2. Objectives

With the above code, we can now easily calculate some quantities of interest. For the sensitivity study, we consider two examples related to plasma-wall interactions. The first is a function related to the peakedness of the heat load profile [9]:

$$\mathcal{I}_1 = \frac{1}{2}\int_{S_t} Q_{\mathrm{o}}^2 d\boldsymbol{\sigma}, \tag{11}$$

with Q_{o} the orthogonal projection of the heat load on the target surface area S_t. This function indicates how good the heat load is distributed over the target surface, and is a possible measure for the performance of a divertor concept. It will further loosely be referred to as the heat load peakedness. The second objective is the outer strike point temperature $\mathcal{I}_2 = T_{\mathrm{os}}$.

3.3. Parameters

In the plasma edge model, several parameters can be considered as uncertain. We will consider four types of uncertain coefficient. The first group consists of the transport coefficients. The anomalous radial transport coefficients D^{i}, ν^{i}, χ^{i}, and χ^{e} are used to simultaneously model classical, neoclassical, and turbulent transport and are amongst the main uncertainties in plasma edge codes. In this simplified neutral model, we additionally include the neutral transport coefficients D_p^{n} and χ^{n}.

The second group are the boundary condition parameters. By including the core input power Q_{c} and n_{c}, we may observe how typical fluctuations in experimental core conditions influence the results. Including the decay lengths $\lambda_{n_{\mathrm{i}}}$ and λ_T on the other hand allows studying the influence of these artificial radial boundary conditions.

Thirdly, we consider the uncertainty on the analytical rate coefficients K_{i}, K_{r}, and K_{cx}. These coefficients exclude non-coronal effects and their sensitivities might therefore indicate the importance of model improvements in this direction. Furthermore, a novel coefficient c_{T} is introduced as a multiplier for the ion temperature in the charge-exchange rate coefficient to capture the influence of isotope effects.

Finally, the equilibrium parameters α, β, γ, and I_{P} are included to consider the impact of changes to the equilibrium parameters.

4. Results and discussion

We now define the model equations

$$\boldsymbol{c}(\boldsymbol{\varphi}, \mathbf{q}) \equiv \boldsymbol{c}_{\mathrm{pe}}(\boldsymbol{\varphi}, \psi(\boldsymbol{\varphi}), \mathbf{q}) = 0 \tag{12}$$

as the plasma state equations from which the magnetic flux ψ is eliminated by using the FBE code that calculates ψ as a function of the input parameters $\boldsymbol{\varphi}$. The equations from section 2 can then be directly applied to obtain the in parts adjoint parameter sensitivities. After solving the model equations, the adjoint plasma edge equations (5) are solved. The directional derivatives can then be evaluated using (8). The choice to reduce the model equations in (12) implies that the sensitivities of the equilibrium calculation are performed using forward finite difference sensitivities. Since such an equilibrium calculation can be done in a couple of seconds, it does also for the equilibrium parameter sensitivities not outweigh the efforts of implementing an adjoint equilibrium calculation [12].

For sake of interpretation, the sensitivities of the reduced objectives $\mathcal{I}_i(\boldsymbol{\varphi}) = \mathcal{I}_i(\boldsymbol{\varphi}, \mathbf{q}(\boldsymbol{\varphi}))$ are normalized as

$$S_{i,j} = \frac{\varphi_{\mathrm{j}}}{\mathcal{I}_i} \frac{d\mathcal{I}_i}{d\varphi_{\mathrm{j}}}. \tag{13}$$

The normalized sensitivities $S_{i,j}$ can then be interpreted as (a linear prediction for) the rate of relative change in objective over the rate of relative change in input parameter. In figure 2, the normalized in parts adjoint sensitivities are given for the heat load peakedness (11) and the outer strike-point temperature with respect to the parameters outlined in section 3. Central finite difference calculations are used to verify the correct implementation of the in parts adjoint method (indicated with diamonds). Although both sensitivity calculations are expected to slightly differ because of discretization, truncation, and cancellation errors, the total error is below one percent for all significant sensitivities ($|S_{i,j}| > 1\%$). Notice that to obtain these central finite difference sensitivities, a total of $2n = 34$ plasma edge simulations is needed in addition to the forward simulation. In contrast, the in parts adjoint sensitivities are obtained at a cost of only $m = 2$ additional adjoint simulations with each a CPU-cost similar to a forward simulation. This highlights again the potential speed-up that can be obtained with the adjoint method.

To interpret the sensitivity values in figure 2, it is important to note that the output uncertainty is determined by both the uncertainty on the input

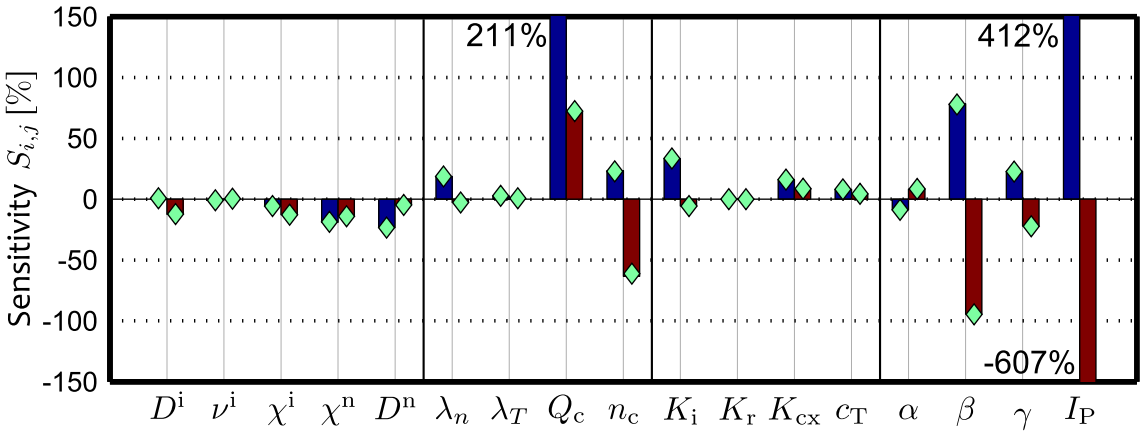

Figure 2: Normalized sensitivities of the heat load objective $\mathcal{I}_1$ (blue) and the outer target strike point temperature $\mathcal{I}_2$ (red) with respect to the uncertain input parameters φ_{i}. Sensitivity values higher than 150% are given explicitly. Diamonds indicate the value of the finite difference validation.

parameters and their propagation to the objectives. As such, it is not necessarily the case that the highest sensitivities indicate the main uncertainty contributions on the objectives. It can for example be observed that both objectives are very sensitive to a change of total toroidal plasma current I_{P}. From the input side, however, the uncertainty on the equilibrium parameters might be several times lower than that on the transport coefficients. The high sensitivities on the magnetic equilibrium parameter indicate though that these parameters should be considered in a UQ study.

Notwithstanding the sensitivity values are local values and as such, dependent on the test case and parameters, several logical trends can be observed in the sensitivity values. For example, negative sensitivities for the radial transport coefficients indicate that enhanced radial particle diffusion ($D^{\mathrm{i}}, D_p^{\mathrm{n}}$) or heat conduction ($\chi^{\mathrm{i}}$,$\chi^{\mathrm{n}}$) logically leads to a less peaked heat load profile and a lower target strike point temperature, at least in the attached divertor conditions of the test case. Furthermore, one can observe that the core parameters Q_{c} and n_{c} play an important role. It should not come as a surprise that increasing the input power increases both the heat load and strike-point temperature.

Other values, like the positive heat load peakedness sensitivity towards K_{i} might be less intuitive. Although the energy losses through ionization goes up for increasing K_{i}, the total outer target heat load increases as well as

the heat load objective $\mathcal{I}_1$. The latter effect can be attributed to the reduced neutral energy convection in this model through the dependence of D_p^{n} on the ionization rate. The sensitivities to the recombination rate K_{r} are very low in these strongly attached plasma conditions, where temperatures are still too high for recombination to play an important role.

5. Conclusions

Quantifying uncertainties on code outputs is an important step for code-based design and scenario development. The high computational cost of plasma edge simulations, however, hinders the application of a true approach to uncertainty quantification. In this paper, an adjoint-based sensitivity approach is therefore proposed for computationally efficient uncertainty propagation. These adjoint-based methods avoid a scaling of the computational cost with the number of uncertain parameters. The in parts adjoint method then avoids the by-hand-linearization of the model equations to the uncertain parameters. Therefore, when an adjoint model of the code is available for optimization studies [9, 10], the parameter sensitivities are readily available.

In the test case, where only 2 objectives are considered, the in parts adjoint method computes the parameter sensitivities at an equivalent computational cost of 2 plasma edge simulations, in comparison to 34 simulation-equivalents for central finite difference calculations. The verification with finite difference calculations furthermore shows a good match between both approaches. Although a relatively simple plasma edge model with fluid neutrals is used, several logical trends can readily be retrieved in the sensitivity values. Whereas magnetic equilibrium calculations are typically dealt with separately from the plasma edge simulation, the high sensitivities to magnetic equilibrium parameters indicate that these parameters should not be excluded from a UQ study.

Finally, it should be noted that this sensitivity study is case-specific and that the sensitivity itself is only locally valid. Therefore, the sensitivity calculation should be repeated for each simulation to know the sensitivities. Future efforts will aim at characterizing the uncertainties and the implementation of sensitivity-based approaches to uncertainty quantification that consider the whole relevant parameter space.

[1] D. Reiter, M. Baelmans, and P. Börner, "The EIRENE and B2-EIRENE codes," *Fusion Science and Technology*, vol. 47, pp. 172–186, Feb 2005.

[2] A. Kukushkin, H. Pacher, V. Kotov, G. Pacher, and D. Reiter, "Finalizing the ITER divertor design: The key role of SOLPS modeling," *Fusion Engineering and Design*, vol. 86, pp. 2865–2873, Dec. 2011.

[3] H. Pacher, A. Kukushkin, G. Pacher, V. Kotov, R. Pitts, and D. Reiter, "Impurity seeding in ITER DT plasmas in a carbon-free environment," *Journal of Nuclear Materials*, vol. 463, pp. 591–595, Aug. 2015.

[4] G. Pacher, H. Pacher, G. Janeschitz, A. Kukushkin, V. Kotov, and D. Reiter, "Modelling of DEMO core plasma consistent with SOL/divertor simulations for long-pulse scenarios with impurity seeding," *Nuclear Fusion*, vol. 47, no. 5, p. 469, 2007.

[5] C. J. Roy and W. L. Oberkampf, "A complete framework for verification, validation, and uncertainty quantification in scientific computing," in *48th AIAA Aerospace Sciences Meeting Including the New Horizons Forum and Aerospace Exposition*, pp. 4–7, 2010.

[6] R. W. Walters and L. Huyse, "Uncertainty analysis for fluid mechanics with applications," tech. rep., 2002.

[7] A. Kukushkin, H. Pacher, G. Janeschitz, D. Coster, D. Reiter, and R. Schneider, "Divertor performance in reduced-technical-objective/reduced-cost ITER," in *26th EPS Conf. on Contr. Fusion and Plasma Physics, Maastricht, 14-18 June 1999*, vol. 23J of *ECA*, pp. 1545–1548, 1999.

[8] Q. Wang, *Uncertainty quantification for unsteady fluid flow using adjoint-based approaches*. PhD thesis, Stanford university, 2009.

[9] W. Dekeyser, D. Reiter, and M. Baelmans, "Divertor target shape optimization in realistic edge plasma geometry," *Nuclear Fusion*, vol. 54, no. 7, p. 073022, 2014.

[10] M. Blommaert, M. Baelmans, W. Dekeyser, N. Gauger, and D. Reiter, "A novel approach to magnetic divertor configuration design," *Journal of Nuclear Materials*, vol. 463, pp. 1220–1224, Aug. 2015.

[11] M. Baelmans, M. Blommaert, J. De Schutter, W. Dekeyser, and D. Reiter, "Efficient parameter estimation in 2D transport models based on

an adjoint formalism," *Plasma Physics and Controlled Fusion*, vol. 56, p. 114009, 2014.

[12] M. Blommaert, H. Heumann, M. Baelmans, N. R. Gauger, and D. Reiter, "Towards Automated Magnetic Divertor Design for Optimal Heat Exhaust," *ESAIM: Proceedings and Surveys*, vol. 53, pp. 49–63, March 2016.

[13] J. Bucalossi, M. Missirlian, P. Moreau, F. Samaille, E. Tsitrone, D. van Houtte, *et al.*, "The WEST project: Testing ITER divertor high heat flux component technology in a steady state tokamak environment," *Fusion Engineering and Design*, vol. 89, pp. 907–912, Oct. 2014.

[14] C. Bourdelle, J. Artaud, V. Basiuk, M. Bécoulet, S. Brémond, J. Bucalossi, *et al.*, "WEST Physics Basis," *Nuclear Fusion*, vol. 55, no. 6, p. 063017, 2015.

[15] M. B. Giles and N. A. Pierce, "An Introduction to the Adjoint Approach to Design," *Flow, Turbulence and Combustion*, vol. 65, no. 3-4, pp. 393–415, 2000.

[16] W. Dekeyser, D. Reiter, and M. Baelmans, "A one shot method for divertor target shape optimization," *PAMM*, vol. 14, no. 1, pp. 1017–1022, 2014.

[17] H. Bufferand, J. Bucalossi, G. Ciraolo, N. Fedorczak, P. Ghendrih, R. Leybros, and others., "Density Regimes and Heat Flux Deposition in the WEST Shallow Divertor Configuration," *Contrib. Plasma Phys.*, vol. 54, pp. 378–382, June 2014.

[18] S. I. Braginskii, "Transport Processes in a Plasma," *Reviews of Plasma Physics*, vol. 1, p. 205, 1965.

[19] W. Dekeyser, D. Reiter, and M. Baelmans, *Optimal Plasma Edge Configurations for Next-Step Fusion Reactors (Optimale plasmarand-configuraties voor nieuwe generatie fusiereactoren)*. PhD thesis, KU Leuven, 2014.

[20] R. Goldston and P. Rutherford, *Introduction to Plasma Physics*. IOP Physics Publishing Ltd., 1995.

[21] V. Rozhansky, S. Voskoboynikov, E. Kaveeva, D. Coster, and R. Schneider, "Simulation of tokamak edge plasma including self-consistent electric fields," *Nuclear Fusion*, vol. 41, no. 4, pp. 387–401, 2001.

[22] H. Heumann, J. Blum, C. Boulbe, B. Faugeras, G. Selig, J.-M. Ané, *et al.*, "Quasi-static free-boundary equilibrium of toroidal plasma with CEDRES++: Computational methods and applications," *Journal of Plasma Physics*, vol. 81, pp. 1469–7807, 6 2015.

[23] H. Grad and H. Rubin, "Hydromagnetic Equilibria and Force-Free Fields," *Proceedings of the 2nd UN Conf. on the Peaceful Uses of Atomic Energy*, vol. 31, p. 190, 1958.

[24] V. D. Shafranov, "Plasma Equilibrium in a Magnetic Field," *Reviews of Plasma Physics*, vol. 2, p. 103, 1966.

[25] J. Blum, *Numerical simulation and optimal control in plasma physics*. Wiley/Gauthier-Villars, 1989.